ELSEVIER

Catalysis Today 50 (1999) 343–352

CATALYSIS TODAY

Ceria films on zirconia substrates: models for understanding oxygen-storage properties

E.S. Putna[a], T. Bunluesin[a], X.L. Fan[a], R.J. Gorte[a,*], J.M. Vohs[a], R.E. Lakis[b], T. Egami[c]

[a]*Department of Chemical Engineering, University of Pennsylvania, Philadelphia, PA 19104, USA*
[b]*LRSM, University of Pennsylvania, PA 19104, USA*
[c]*Department of Materials Science and Engineering, University of Pennsylvania, Philadelphia, PA 19104, USA*

Abstract

The oxygen-storage properties of ceria in three-way automotive catalysts are promoted and stabilized by mixing with zirconia. In the present study, this promotion was investigated using model catalysts in which ceria films were vapor deposited onto α-Al_2O_3, polycrystalline ZrO_2, polycrystalline Y_2O_3-stabilized ZrO_2 (YSZ), and YSZ(1 0 0), (1 1 1), and (1 1 0) single crystals. Following deposition of Pd, both TPD of CO and steady-state CO-oxidation kinetics suggest that the ceria films on the zirconia-based substrates were much more easily reduced than films on α-Al_2O_3. Polycrystalline zirconia and YSZ and the YSZ single crystals were equally effective in promoting ceria reducibility. Structural studies of ceria on YSZ(1 0 0), using both TEM and EDSXD (energy-dispersive, surface X-ray diffraction), demonstrate that ceria forms ordered overlayers on YSZ(1 0 0), oriented with respect to the YSZ surface. The lattice parameter for ceria is decreased by only 0.6% compared to bulk CeO_2, but the coherence length suggests that the overlayer may have a high defect density. It is suggested that the structure-directing properties of zirconia are responsible for the enhanced properties of ceria–zirconia mixed oxides.

Keywords: YSZ; Ceria; Oxygen-storage properties; Zirconia; CO-oxidation

1. Introduction

Ceria is an important component in automotive, emissions-control catalysis, primarily because of its ability to store and release oxygen [1–8]. This oxygen-storage capacity (OSC) is crucial for controlling the ratio of oxidants and reductants in the exhaust, so that CO and hydrocarbons can be oxidized simultaneously with the reduction of NO. However, the OSC of pure ceria is known to degrade with time in the automotive exhaust environment, so that ceria is usually included as a mixed oxide with zirconia, which stabilizes oxygen-storage properties of ceria [9–18]. The details of how ceria performs its role as an oxygen-storage component and the mechanism by which zirconia stabilizes the redox properties of ceria are not well understood. Developing a better understanding of these issues was the primary goal of the present investigation.

First, it is important to consider how ceria performs its role in oxygen storage. It is widely recognized that

*Corresponding author. Tel.: +1-215-898-4439; fax: +1-215-573-2093; e-mail: gorte@home.seas.upenn.edu

0920-5861/99/$ – see front matter
PII: S0920-5861(98)00514-8

the reduction of ceria is facilitated by contact between ceria and a precious metal and requires the presence of reducing agents (CO, H_2, or hydrocarbons). While the utilization of oxygen from ceria is most often studied by transient measurements such as temperature-programmed reduction, it can also be observed in steady-state rate measurements. For example, under reducing conditions, ceria-supported metals are able to catalyze oxidation reactions through a mechanism in which oxygen from ceria reacts with CO or hydrocarbons adsorbed on the precious metals [19–25]. In the case of CO oxidation, this leads to a second rate process for ceria-supported catalysts, which is zeroth-order in CO and has an activation energy of 14 kcal/mol [21–23]. For comparison, rates on alumina-supported, precious metals are inverse first-order in CO and exhibit an activation energy of 26 kcal/mol. Similar mechanistic steps appear to be responsible for the fact that ceria-supported metals exhibit much higher rates than their alumina-supported counterparts for both the water–gas shift and methane–steam-reforming reactions [24,25].

As mentioned earlier, the high-temperature environment in the catalytic converter results in deactivation of the OSC component. Because the loss of OSC is accompanied by an increase in ceria crystallite size, it has been suggested that the loss is due to a decrease in the interfacial contact between ceria and the precious metals [6]. However, it has recently been shown that other factors may also be involved [19,23–25]. In experiments using model catalysts prepared by vapor deposition of catalytic metals onto ceria films which had been previously calcined to various temperatures, it was demonstrated that oxygen transfer from ceria to the supported metals depended significantly on the calcination temperature. For Rh or Pd supported on CeO_2 single crystals and ceria films which had been calcined to high temperatures (>1270 K), CO TPD studies showed minimal reaction to CO_2 [19,20]. This result is significantly different from that obtained for catalysts prepared from ceria films calcined at lower temperatures. Furthermore, in steady-state measurements, the ceria-mediated processes for CO oxidation, for the water–gas shift reaction, and for the methane–steam-reforming reaction were absent on catalysts prepared using ceria films calcined at high temperatures [23–25]. Finally, model catalysts prepared by addition of Pd to mixed oxides of ceria and zirconia were found to maintain the ceria-mediated process for CO oxidation to much higher calcination temperatures than catalysts prepared from ceria alone [23].

The reason why high-temperature calcination affects ceria and its ability to release oxygen remains uncertain. In recent TPD studies, it has been shown that a weakly bound form of oxygen exists on vapor-deposited ceria films on α-Al_2O_3(0 0 0 1), but is absent on a CeO_2(1 1 1) surface [26]. It has been demonstrated that this oxygen, which desorbs between 800 and 1200 K, reacts with CO to form CO_2 in TPD studies from supported Rh particles. The nature of this oxygen is unknown, although it is clearly part of the ceria lattice. Calculations imply that the active oxygen may be associated with very small crystallites or with certain crystal facets [27]. The amount of weakly bound oxygen observed in TPD increases significantly if the ceria film is supported on zirconia [28].

One of the difficulties in understanding how zirconia stabilizes the OSC of ceria is that ceria–zirconia mixed oxides used for oxygen storage are complex materials. While these are sometimes considered to be solid solutions of ceria and zirconia, recent neutron diffraction studies indicate that this is not the case for materials optimized for OSC [29]. This observation suggests that the role of zirconia may be to control the structure or the size of the ceria crystallites. Indeed, in a preliminary study of thin ceria films on single crystals of yttria-stabilized zirconia (YSZ), it was shown that ceria films form ordered overlayers [30–34]. On YSZ(1 0 0), for example, 4 nm thick, ceria films form epitaxial islands, in the $\langle 1\,0\,0 \rangle$ direction, with a nearly relaxed lattice constant [30,31]. Similar results are found for YSZ(1 1 1) and YSZ(1 1 0) [33,34].

The single-crystal results are intriguing since model catalysts based on these well-defined systems can be characterized in much greater detail and therefore have the potential to provide insights into the nature of ceria–zirconia mixed oxides and the reasons for their enhanced stability compared to pure polycrystalline ceria. In the present study, the ability of various model ceria catalysts to supply oxygen to reactants adsorbed on supported metals was studied using TPD of CO and measurements of steady-state, CO-oxidation rates. The structure of ceria films on the single-crystal, YSZ supports was examined using TEM and energy-dispersive, X-ray surface scattering.

2. Experimental

The equipment and experimental methods used for the TPD measurements have been described previously [35,36]. Briefly, the single-crystal, YSZ(1 0 0) (Aithaca Chemical, 8 mol% Y) and α-Al_2O_3(0 0 0 1) substrates were mounted on tantalum foils, which allowed the crystals to be heated or cooled over a wide temperature range. The temperature was monitored using a chromel–alumel thermocouple attached to the back surface using a ceramic adhesive (Aremco 516). Ion bombardment was used to clean the samples until no impurities were detected by Auger electron spectroscopy (AES). The crystals were then heated in 10^{-7} Torr of O_2 for 10 min at 800 K and for 30 min at 450 K to reoxidize and to anneal out defects. TPD measurements were carried out with a linear heating rate of 12 K/s.

Ceria and Pd were added to the substrates by vapor deposition. For ceria, Ce metal (Johnson Matthey, 99.9%) was deposited while holding the substrate at 450 K in the presence of 10^{-7} Torr of O_2. The samples were then annealed at 450 K for an additional 15 min in 10^{-7} Torr of O_2 to ensure complete oxidation to CeO_2. Pd deposition was carried out in vacuum with the substrate held at 300 K. In the present study, a ceria coverage of 1×10^{16} CeO_2/cm^2, and a Pd coverage of 2×10^{15} Pd/cm^2 were used, as determined by a film-thickness monitor [36].

The samples used in the steady-state rate measurements were prepared in a manner similar to that described above, using the following supports: a polycrystalline α-Al_2O_3 plate (Coors), a YSZ(1 0 0) single crystal, a polycrystalline zirconia film, and a polycrystalline YSZ film (8 mol% Y). The polycrystalline films were prepared by spray pyrolysis of aqueous solutions of the appropriate nitrates ($ZrO(NO_3)_2{\cdot}xH_2O$ and $Y(NO_3)_3{\cdot}xH_2O$, both 99.9%, Johnson Matthey) in air on α-Al_2O_3 plates at 600 K to form films approximately 20 μm thick. The support films were then calcined in air at 900 K for an additional hour. The polycrystalline ZrO_2 film was shown by XRD to be predominately monoclinic, while the polycrystalline YSZ film was cubic. Following vacuum deposition of ceria and Pd, the samples were placed in a quartz, tubular reactor for measuring CO oxidation rates, as described elsewhere [21]. The conversion was monitored using an on-line GC equipped with a methanator and an FID detector. Conversion of the limiting reagent was usually below 1%, so that differential conditions were maintained. In the absence of Pd, rates were undetectable for these conditions. All reported rates were normalized to the external planar surface area of the substrates.

The X-ray scattering experiments were performed at the National Synchrotron Light Source, Brookhaven National Laboratory, beam line X-7A, using energy-dispersive, surface X-ray diffraction (EDSXD) [30,31]. The samples were prepared by vapor deposition of Ce metal onto YSZ(1 0 0), as described above, with the additional calcination described in Section 3 being performed in air. In the EDSXD experiment, a white beam of synchrotron radiation was directed toward the sample surface at an incident angle of 0.3°, an angle only slightly above the critical angle for total reflection for the energy range used, 15–40 keV. The scattered X-rays were then detected by an energy-sensitive detector placed at a 2θ of 25°. Because the wavevector of diffracted X-rays is related to the energy of the X-rays, the energy spectrum of the scattered X-rays is composed of the diffraction pattern as well as fluorescence lines. Furthermore, the energy spectra as a function of sample orientation provide a two-dimensional diffraction pattern. Therefore, EDSXD provides detailed structural information for the thin ceria films.

TEM samples were prepared by thinning a YSZ(1 0 0) crystal using a 600-grit sandpaper to a thickness of ∼150 μm, followed by dimpling with a grinding wheel to a thickness of ∼40 μm [36]. The dimpled YSZ sample, held at 78 K, was then ion milled to perforation using Ar^+ ions, resulting in an average sample thickness of ∼25 nm. After ion milling, the YSZ crystal was annealed at 1470 K overnight to eliminate defects introduced by the thinning process. Following TEM characterization of the annealed YSZ sample, Ce metal was deposited onto the YSZ, followed by calcination in air to 1020 K for 2 h. TEM and TED experiments were carried out on a Philips EM 400T, operated at 120 kV, and a JEOL 4000EX operated at 400 kV.

It is important to point out that the pretreatment conditions used in this study for the ceria films on zirconia were mild enough to prevent formation of solid solutions of ceria and zirconia. The results of the EDSXD, TEM, and AES experiments were all con-

sistent with ceria remaining at the surface under all calcination conditions used in this study.

3. Results

3.1. EDSXD results

The results from structural characterizations of ceria films on YSZ(1 0 0) have been described in more detail elsewhere [30,31], with results from the YSZ(1 1 0) and YSZ(1 1 1) reported separately [33,34]. After cerium vapor deposition and exposure to air, an as-deposited ceria film showed no detectable diffraction pattern, suggesting that the film was composed of an amorphous oxide or hydroxide of Ce. Heating in air transformed the film to CeO_2 and formed a crystalline, epitaxial structure, partially coherent with the YSZ(1 0 0) lattice. This process began at approximately 670 K. A typical energy spectrum of the scattered X-rays along the [1 0 0] direction is shown in Fig. 1 for calcination at 770 K. YSZ and CeO_2 Bragg peaks for the (2 0 0), (4 0 0), (6 0 0), and (8 0 0) planes are clearly observable. Also present are fluorescence lines for Y, Zr, and Ce. From this spectrum, one can determine that the lattice constant for the ceria film is 5.38 Å, which is 0.6% smaller than the value for bulk ceria, 5.4113 Å. The lattice constant of the YSZ crystal was found to be 5.129 Å, in reasonable agreement with the reported value of 5.131 Å.

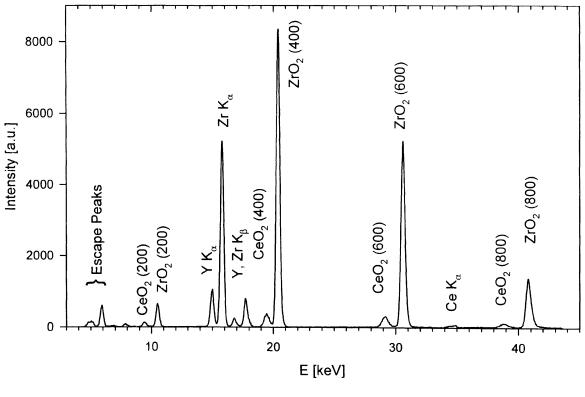

Fig. 1. EDSXD spectrum for a ceria overlayer on YSZ(1 0 0), taken along the [1 0 0] direction after calcination in air to 770 K. The spectrum shows the diffraction pattern for the overlayer, as well as fluorescence lines from Y, Zr, and Ce.

A close examination of the diffraction features along different lattice directions, provides additional information on the ceria film. Based on these results, there appears to be a slight mismatch in the angular orientation of the CeO_2 and YSZ, $\sim 0.1^\circ$, which may help to reduce strain in the CeO_2 layer. The domain size for the CeO_2 film, determined from the peak width, ranged from 4 to 8 nm, depending upon the annealing conditions. The grains were observed to grow in size with heating, but never exceeded 8 nm. All of these grains had the same orientation, but were laterally displaced by a random amount, so that they are translationally incoherent, even though they are orientationally coherent. The results for the (1 1 0) and (1 1 1) surfaces were very similar. In each case, semicoherent, epitaxial CeO_2 films were found, oriented in the direction of the YSZ crystals on which they were formed, with grain sizes ranging from 4 to 8 nm.

3.2. TEM of CeO_2/YSZ(1 0 0)

TEM provided information on the ceria films which was highly complementary to the EDSXD results. The sample examined by TEM consisted of a ceria film on a thinned YSZ(1 0 0) crystal, which was annealed in air to 1020 K, a temperature which may have resulted in some loss of the ceria by dissolution. Damage to the YSZ crystal from processing was not apparent in the micrographs, and large regions of uniform lattice were observable by routine phase-contrast imaging. As shown in Fig. 2(a), the ceria was present as isolated and connected islands, with an average size of approximately 50 nm. In general, the particles were nearly square, with a rectangular aspect ratio of 1.2. For most particles, a Moiré-fringe effect was observed. These fringes are the result of two superimposed lattices with similar periodicities, indicating that the CeO_2(1 0 0) particles have formed in epitaxy with the YSZ(1 0 0). The spacing of the Moiré fringes are related to the unit cell dimensions of the superimposed lattices and their relative rotation. Fig. 2(b) contains one ceria domain which, by selected area diffraction, was found to have no rotation relative to the YSZ substrate. The Moiré-fringe spacing was 54 Å. If the lattice parameter of YSZ is taken to be 5.131 Å, the lattice parameter for the CeO_2 film can be calculated to be 5.386 Å, in good agreement with the results from EDSXD.

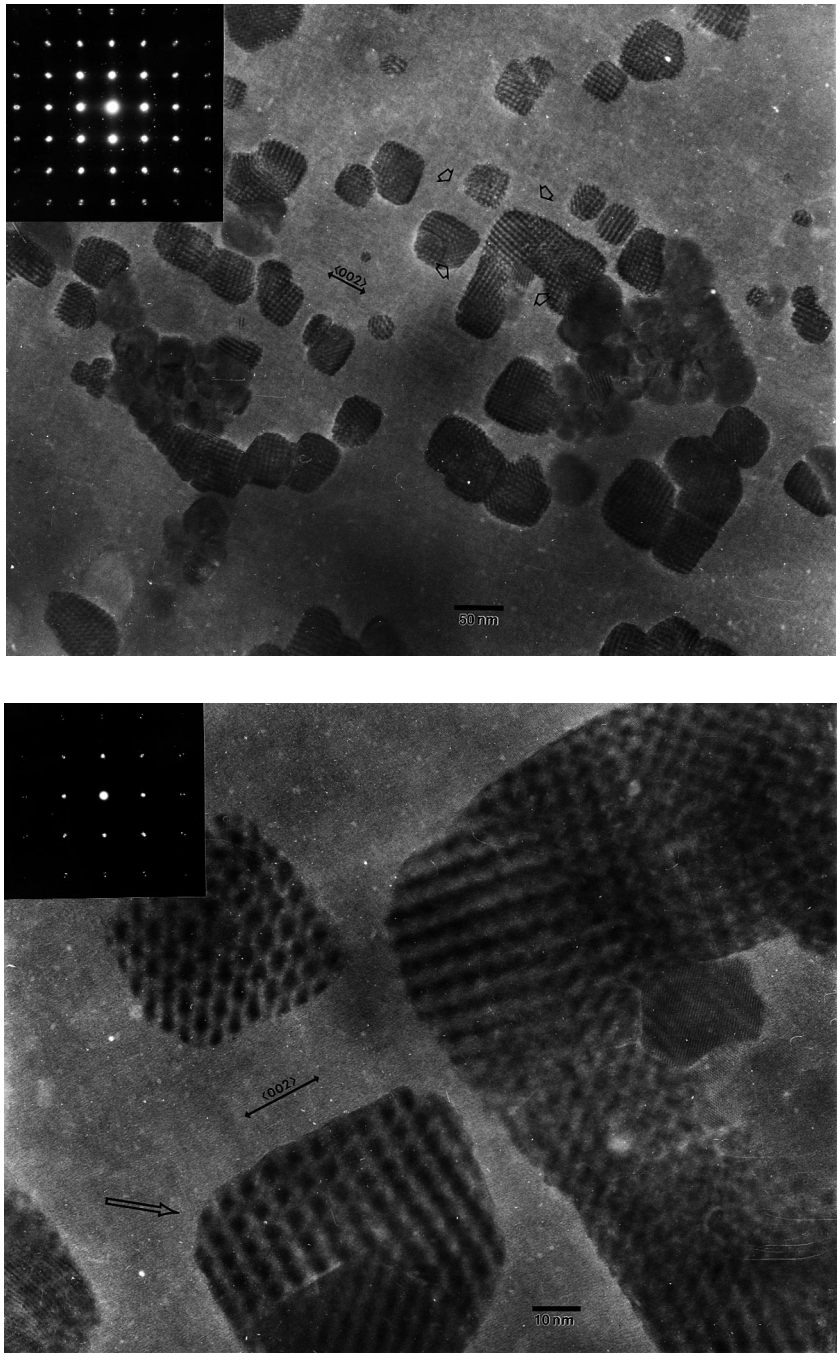

Fig. 2. TEM results for a ceria film on YSZ(1 0 0) after heating to 1020 K in air. The results in (b) are from the same region as (a), except that a higher magnification was used of the region shown in arrows. The line in (b) gives the [1 0 0] direction.

An apparent discrepancy exists between the TEM and EDSXD results for the domain size of the CeO_2 particles. Based on EDSXD, the domain size was estimated to be 8 nm, while the particle size measured in TEM was almost an order of magnitude larger. This may be due to the differences in the sample preparation conditions, such as the temperatures used in the calcination of the samples. Alternatively, this may imply that, on a short-range scale, the particles contain defects which are not apparent based on the long-range order observed from the Moiré fringe in TEM. Because defects could be crucial in the transfer of oxygen from ceria, this issue needs to be examined in more detail.

3.3. UHV adsorption studies

In previous studies on ceria-supported metals, it was shown that the structure of ceria strongly affects its reducibility during TPD of CO from supported metals [19,20]. For Pt, Pd, or Rh on polycrystalline ceria which had been calcined at temperatures less than 1070 K, a significant fraction, up to ~30%, of the CO was oxidized to CO_2. However, for CeO_2(1 1 1) and CeO_2(1 0 0) single crystals and for polycrystalline films calcined at higher temperatures, a negligible fraction of CO adsorbed on supported metals reacted to CO_2 during TPD. Finally, for ceria films formed by vapor deposition onto an α-Al_2O_3(0 0 0 1) crystal, some CO_2 was formed during TPD of CO from supported metals, but the results indicated that only a small fraction of the ceria, ~20%, underwent reduction [26]. A significantly higher extent of ceria reduction was possible for a ceria film deposited on polycrystalline zirconia [28].

The TPD results for CO from Pd particles deposited on ceria films on YSZ(1 0 0) are shown in Fig. 3 and demonstrate that these ceria films are highly reducible. CO desorbed in a peak centered at 500 K with a shoulder to lower temperatures, while CO_2 desorbed between 350 and 550 K. (The small CO_2 peak between 550 and 600 K appears to result from a carbonate, possibly associated with an impurity, as discussed elsewhere [37].) The ratio of the CO and CO_2 peak areas was roughly 1:1, indicating that ~50% of the adsorbed CO reacted to CO_2 in the initial desorption measurement. This fraction is considerably higher

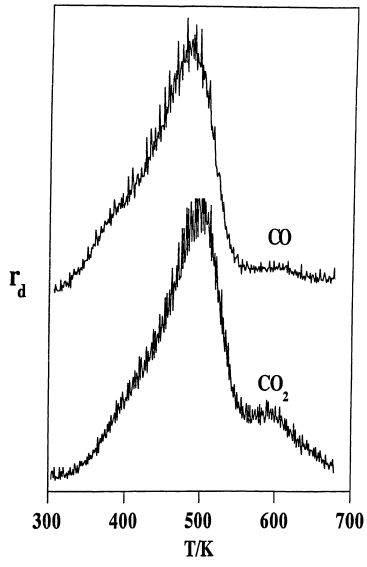

Fig. 3. TPD curves following CO adsorption on Pd particles supported on a ceria film on YSZ(1 0 0). The ceria film was prepared by vapor deposition of Ce in 10^{-7} Torr of O_2, after which the ceria film was heated in O_2 to 450 K. Pd was deposited in vacuum at 300 K and the sample exposed to CO without any exposure to O_2. The rate of desorption (r_d) was monitored using the partial pressures of CO and CO_2. The results demonstrate that oxygen from the oxidized ceria film can react with CO adsorbed on the Pd particles.

than we observed on any of the pure ceria substrates. In subsequent TPD measurements, the amount of CO which reacted to CO_2 decreased, implying that the ceria film became reduced. It should be noted that no CO_2 was observed in TPD studies in which Pd or other metals were deposited directly on either α-Al_2O_3 or YSZ, in the absence of ceria [38–40]. Finally, CO desorption results for Pd/ceria films on YSZ(1 1 1) and YSZ(1 1 0) were identical to those shown here for YSZ(1 0 0).

The most significant conclusion to be reached from these results is that ceria films deposited onto YSZ single crystals are much more reducible than ceria films prepared in an identical manner on α-Al_2O_3(0 0 0 1), even though the ceria films on YSZ are highly oriented in low-index directions. The orientation of the YSZ crystal does not seem to be important in determining its ability to promote CO_2 formation during CO desorption measurements on ceria-supported metals.

3.4. CO oxidation rates

As discussed in Section 1, evidence for a ceria-mediated mechanism during steady-state CO oxidation has been observed for polycrystalline ceria-supported metals [21–23]. This second process can be identified by the fact that the rates are zeroth-order in CO, as compared to the inverse first-order rates observed on precious metals alone, and show a much lower activation energy, 14 kcal/mol compared to 26 kcal/mol. Of special importance for our purposes here, intentional deactivation of ceria by high-temperature calcination, prior to addition of the metal, significantly decreased the rates associated with the ceria-mediated process [19,23]. This implies that utilization of the oxygen in the oxide can be monitored through CO oxidation rates.

Fig. 4 shows the rates for CO oxidation measured as a function of CO pressure at 515 K on each of the model supports, following vapor deposition of Pd. The O_2 pressure for these measurements was fixed at 0.3 Torr. For Pd on a zirconia film, only the inverse first-order rate process, associated with Pd alone, was observed. The rates are only shown for CO pressures below 10 Torr because the rates were too low to measure at higher CO pressures. The observation of inverse first-order rates with respect to CO is expected since zirconia is expected to be irreducible. One observes similar results for Pd/α-Al_2O_3 [23], so that the data here provide a baseline for the activity of the catalytic metal alone. Because CO oxidation on Pd is structure-insensitive, the magnitude of the rates provides an estimate of the Pd surface area. Together with the Pd coverage, the area can be used to calculate an average particle size, ~6 nm.

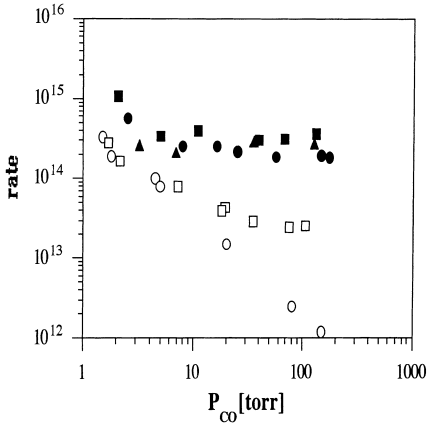

Fig. 4. Differential reaction rates for CO oxidation as a function of CO pressure at 515 K and a fixed O_2 pressure of 0.3 Torr. The rates are in molecules/cm^2 s. Results shown are for the following samples: Pd/α-Al_2O_3 (○), Pd/ceria/α-Al_2O_3 (□), Pd/ceria/polycrystalline zirconia (▲), Pd/ceria/polycrystalline YSZ (●), and Pd/ceria/YSZ(1 0 0) (■).

For the ceria/α-Al_2O_3 support, prepared by vapor deposition of ceria, followed by deposition of Pd, there is evidence for the ceria-mediated mechanism through a zeroth-order process at the higher CO pressures; however, the rates of the zeroth-order process are quite low, $\sim 3\times10^{13}$ CO_2/s cm^2. This observation of low CO-oxidation rates at high CO pressures is consistent with our earlier TPD results which showed that ceria films vapor deposited onto a sapphire crystal are relatively irreducible [28]. Based on oxygen isotope exchange in the TPD studies, only approximately 20% of the ceria film on the sapphire support undergoes reduction. The ceria-mediated process is much more evident for the supports prepared by vapor deposition of CeO_2 on zirconia, followed by deposition of Pd. The rates for the zeroth-order process were between 2×10^{14} and 3×10^{14} CO_2/s cm^2 on all of the zirconia substrates, which is almost an order of magnitude higher than was observed for Pd on the ceria/α-Al_2O_3 counterparts. The inverse first-order process is not observed for the ceria/zirconia supports under the conditions of these measurements.

While it is possible that some of the differences between ceria/zirconia and ceria/α-Al_2O_3 could be due to metal particle size, we feel it is unlikely that there are drastic differences for the Pd on these supports. Previous work for catalysts prepared by vapor deposition of 2×10^{15} Pd/cm^2, with similar pretreatment conditions, suggests that the Pd particle sizes are approximately 6 nm on each of the supports [23]. Since in the Auger electron spectra of the ceria films the peaks due to the underlying support were completely obscured by ceria, the contact between ceria and Pd must be approximately the same on each of the catalysts. A more likely explanation for the differences between the catalysts prepared from ceria films on either the zirconias or the α-Al_2O_3 is that structural differences in the ceria affect its reducibility. As discussed previously, ceria structure has been shown to significantly affect the ceria-mediated rates

observed on Pd/ceria catalysts. The present results confirm those conclusions.

Finally, it should be noted that the CO oxidation rates for the ceria-mediated process are about the same for each of the zirconia-based supports, whether the zirconia was pure and monoclinic or yttria-stabilized in the cubic form. Because the cubic form of zirconia has a significantly higher oxygen-ion conductivity, it would appear that ionic conductivity of the support is not the critical factor. The CO oxidation rates were also the same on the single-crystal, YSZ-supported Pd/ceria sample as on the polycrystalline YSZ support, implying that the orientation of the ceria particles is unlikely to be the critical factor. Therefore, the structural changes which zirconia induces in ceria and which are responsible for the enhanced reducibility of zirconia-supported ceria are not due to preferential orientation of the ceria surface.

4. Discussion

As discussed in previous papers [19,23,24], the reducibility of ceria is highly structure-sensitive, although the reasons for this are not understood. Based on bulk thermodynamics, ΔH for the reaction $4CeO_2 \rightarrow 2Ce_2O_3 + O_2$ is 178 kcal/mol. However, TPD studies of O_2 from ceria films on zirconia and small ceria crystallites on alumina suggest that 60 kcal/mol is a more reasonable estimate for the binding energy of oxygen on the active form of ceria [26]. One possibility for the lower binding energy on active forms of ceria is that structural changes which occur upon reduction of bulk CeO_2, which is cubic, to bulk Ce_2O_3, which is hexagonal, do not occur upon reduction of the active form of ceria. Indeed, others have reported evidence for stable, cubic phases of Ce_2O_3 [41,42]. Another possibility is that small ceria crystallites do not have crystallographic structures identical to that of bulk ceria [27] and may be much easier to reduce [43]. Whatever the explanation for the ease with which small ceria crystallites undergo reduction, it must be recognized that large ceria crystals, CeO_2(1 1 1), and CeO_2(1 0 0), are essentially inactive and hard to reduce [19,20].

The work described in this paper demonstrates that ceria films on zirconia substrates are highly reducible, much more so than ceria films on α-Al_2O_3. The ease of ceria reduction, and the ability to use the oxygen from this reduction, was demonstrated in both the transient and steady-state oxidation of CO adsorbed on supported Pd particles. The particular structure of the zirconia (monoclinic or cubic) and orientation of the YSZ substrate ((1 0 0), (1 1 0), or (1 1 1)) does not appear to be important for imparting improved reductive properties to ceria. Furthermore, zirconia affected the ceria, even though zirconia was essentially buried far below the surface in our studies. No evidence for the formation of a ceria–zirconia mixed oxide was observed under the conditions of our work. Therefore, under the conditions of our study, the effect of zirconia must be that of a structural promoter, one which promotes the formation of an easily reducible form of ceria.

One can envision a number of ways in which zirconia and YSZ could influence the structure of ceria and therefore its reducibility. First, interactions with the zirconia may simply promote the formation of small, incoherently displaced islands of ceria. While the CeO_2 films in our study grew epitaxially on the surface of the single-crystal YSZ, the films were translationally incoherent with respect to the zirconia, even though the lattice constant for the films differed from that of bulk ceria by only 0.6%. Normally, when the lattice mismatch is this small and the cohesion strong enough to induce epitaxy, very thin films tend to be perfectly coherent, so that the film has the same lattice constant as the substrate. For thick films on the other hand, the strain is usually relaxed by interfacial mismatch dislocations. However, for ceria on YSZ, it appears that the interface between ceria and zirconia is not strong enough to support the mismatch strain and the films were too thin to support mismatch dislocations. The mismatch simply produced incoherently displaced islands. Island formation could explain the increased reducibility of ceria, since a ceria substrate with more defects, including increased numbers of grain boundaries and oxygen vacancies, should undergo reduction and transport oxygen more easily than will a highly ordered ceria crystal.

Alternatively, the YSZ substrate could affect the stability and structure of the reduced ceria. For example, if reduced ceria were maintained in the cubic structure by zirconia, the energy difference between oxidized and reduced forms of ceria could be strongly modified [41]. In the present studies, we were unable

to examine the structure of reduced films, but this will be an important goal in future work.

While not the main focus of the present investigation, it should be mentioned that, in addition to the formation of more structurally active ceria sites as a result of zirconia contact, zirconia imparts added thermal stability to supported ceria catalysts. Previously, CO oxidation studies have shown that, following high-temperature calcination, ceria–zirconia model catalysts show higher activities toward promotion of the ceria-mediated mechanism than did ceria samples [23]. Thus, it appears that zirconia helps to promote the oxygen-storage capacity (OSC) of ceria in an automotive emissions catalytic converter by promoting the formation and the stabilization of more active ceria sites than those present for bulk ceria.

5. Summary

The present work has demonstrated that ceria films on zirconia are more reducible and have a higher activity towards promotion of the ceria-mediated oxidation of CO on supported metals than do ceria films on alumina. The enhanced activity and thermal stability of the ceria–zirconia samples appear to result primarily from structural modification of the ceria in contact with the zirconia.

Acknowledgements

This work was supported by the Department of Energy, Office of Basic Energy Sciences, grant no. DE-FG03-85-13350 (RJG) and grant no. DE-FG02-96ER14682 (JMV and TE). Some facilities used in this work were also partially funded by the National Science Foundation through the MRSEC program (grant no. DMR-963298).

References

[1] R.W. McCabe, J.M. Kisenyi, Chem. Ind. 15 (1995) 605.
[2] K. Otsuka, M. Hatano, A. Morikawa, J. Catal. 79 (1983) 493.
[3] H.S. Gandhi, M. Shelef, Stud. Surf. Sci. Catal. 30 (1987) 199.
[4] R.K. Herz, J.A. Sell, J. Catal. 94 (1985) 199.
[5] G.B. Fisher, J.R. Theis, M.V. Casarella, S.T. Mahan, SAE Paper 931034 (1993).
[6] J.G. Nunan, H.J. Robota, M.J. Cohn, S.A. Bradley, J. Catal. 133 (1992) 309.
[7] M. Shelef, G.W. Graham, Catal. Rev.-Sci. Eng. 36 (1994) 433.
[8] A. Trovarelli, Catal. Rev.-Sci. Eng. 38 (1996) 439.
[9] M. Ozawa, M. Kimura, A. Isogai, J. Alloys Comp. 193 (1993) 73.
[10] G. Balducci, J. Kaspar, P. Fornasiero, M. Graziani, M.S. Islam, J. Phys. Chem. B 102 (1998) 557.
[11] G. Vlaic, P. Fornasiero, S. Geremia, J. Kaspar, M. Graziani, J. Catal. 168 (1997) 386.
[12] G.R. Rao, J. Kaspar, S. Meriani, R. Dimonte, M. Graziani, Catal. Lett. 24 (1994) 107.
[13] P. Fornasiero, R. Dimonte, G. Ranga Rao, J. Kaspar, S. Meriani, A. Trovarelli, M. Graziani, J. Catal. 151 (1995) 168.
[14] M. Haneda, K. Miki, N. Kakuta, A. Ueno, S. Tani, S. Matsura, M. Sato, Nihon Kagaku Kaishi (1990) 820.
[15] T. Ohata, Rare Earths 17 (1990) 37.
[16] J.G. Nunan, W.B. Williamson, H.J. Robota, SAE Paper 960768 (1996).
[17] S. Otsuka-Yao, H. Morikawa, N. Izu, K. Okuda, J. Jpn. Inst. Metals 59 (1995) 1237.
[18] M.H. Yao, T.E. Hoost, R.J. Baird, F.W. Kunz, J. Catal. 166 (1997) 67.
[19] H. Cordatos, T. Bunluesin, J. Stubenrauch, J.M. Vohs, R.J. Gorte, J. Phys. Chem. 100 (1996) 785.
[20] J. Stubenrauch, J.M. Vohs, J. Catal. 159 (1996) 50.
[21] T. Bunluesin, H. Cordatos, R.J. Gorte, J. Catal. 157 (1995) 222.
[22] T. Bunluesin, E.S. Putna, R.J. Gorte, Catal. Lett. 41 (1996) 1.
[23] T. Bunluesin, R.J. Gorte, G.W. Graham, Appl. Catal. B 14 (1997) 105.
[24] T. Bunluesin, R.J. Gorte, G.W. Graham, Appl. Catal. B 15 (1998) 107.
[25] R. Craciun, B. Shereck, R.J. Gorte, Catal. Lett. 51 (1998) 149.
[26] E.S. Putna, J.M. Vohs, R.J. Gorte, J. Phys. Chem. 100 (1996) 17862.
[27] H. Cordatos, D. Ford, R.J. Gorte, J. Phys. Chem. 100 (1996) 18128.
[28] E.S. Putna, J.M. Vohs, R.J. Gorte, Catal. Lett. 45 (1997) 143.
[29] T. Egami, W. Dmowski, R. Brezny, SAE Paper 970461 (1997).
[30] W. Dmowski, T. Egami, R. Gorte, J. Vohs, Physica B 221 (1996) 420.
[31] W. Dmowski, E. Mamontov, T. Egami, S. Putna, R. Gorte, Physica B 248 (1998) 95.
[32] W. Dmowski, S. Fu, T. Egami, R. Gorte, J. Vohs, Mater. Res. Soc. Conf. Proc. 401 (1996) 115.
[33] W. Dmowski, T. Egami, R. Gorte, J. Vohs, Catalyst materials for high-temperature processes, Ceramic Trans. 73 (1997) 113.
[34] W. Dmowski, E. Mamontov, T. Egami, S. Putna, R.J. Gorte, Physica B 248 (1998) 95.

[35] E.I. Altman, R.J. Gorte, J. Catal. 113 (1988) 185.
[36] S. Roberts, R.J. Gorte, J. Phys. Chem. 93 (1990) 5337.
[37] E.S. Putna, J.M. Vohs, R.J. Gorte, G.W. Graham, Catal. Lett. 54 (1998) 17.
[38] H. Cordatos, T. Bunluesin, R.J. Gorte, Surf. Sci. 323 (1995) 219.
[39] G. Zafiris, R.J. Gorte, J. Catal. 132 (1991) 275.
[40] E.S. Putna, R.J. Gorte, J.M. Vohs, G.W. Graham, J. Catal. 178 (1998) 598.
[41] J.C. Conesa, Surf. Sci. 339 (1995) 337.
[42] T.X.T. Sayle, S.C. Parker, C.R.A. Catlow, Surf. Sci. 316 (1994) 329.
[43] Y.-M. Chiang, E.B. Lavik, I. Kosacki, H.L. Tuller, J.Y. Ying, J. Electroceramics 1 (1997) 7.